Finite-Element Analysis of Temperature Rise and Lesion Formation from Catheter Ultrasound Ablation Transducers

Kenneth L. Gentry, Mark L. Palmeri, *Student Member, IEEE*, Nasheer Sachedina, and Stephen W. Smith, *Member, IEEE*

***Abstract*—A model using finite-element analysis (FEA) has been developed to calculate the temperature rise in tissue from intracardiac ultrasound ablation catheters and to predict if this temperature rise is adequate for producing a lesion in the tissue. In the model, acoustic fields are simulated with Field II, and heat transfer is modeled with an FEA program. To validate the model, we compare its results to experimental results from an integrated, real-time three-dimensional (3-D) ultrasound imaging and ultrasound ablation catheter. The ultrasound ablation transducer is a ring transmitting at 10 MHz capable of producing an acoustic intensity of 16 W/cm^2. It was used to ablate four lesions in tissue, and temperature rise as a function of time was monitored by embedded thermocouples. The average absolute difference between final temperatures predicted by FEA and those measured is 1.95 ± 0.72°C. Additionally, model and experimental lesion size are in good agreement. The model then is used to design a new ultrasound catheter with a 7.5 MHz linear phased array for ablation. Eight designs are modeled, and acoustic intensity, temperature rise, and ablation ability are compared.**

I. Introduction

With the feasibility of catheter-delivered ultrasound for ablation of cardiac tissue well established [1]–[4], mathematical models for lesion creation are needed to ensure both the safety and efficacy of the lesion-creation procedure. Many models exist for the temperature rise associated with the absorption of an acoustic beam in tissue. For simple sound field geometries, analytic methods may be used [5], [6]. When the geometry of the tissue or the sound field becomes too complex, it becomes necessary to find numerical solutions by using the finite difference method [7], [8] or finite-element analysis (FEA) [9]. Lesion size then can be estimated using calculated temperature data.

Our goal is integrated real-time three-dimensional (3-D) ultrasound imaging [10], [11] and ultrasound ablation in the same intracardiac catheter (Fig. 1). A 2-D array at the distal tip of the catheter is used for imaging the heart and aiding placement of a lesion created by one or more ablation elements, also at the tip of the catheter. Myocardial lesions are useful in the treatment of atrial fibrillation and other cardiac arrhythmias [12], and intracardiac echocardiography can provide views of the heart anatomy better than, or not available to, conventional transthoracic echocardiography [13], [14]. Real-time, 3-D intracardiac echocardiography catheters have visualized heart anatomy and been used to guide a number of surgical procedures in vivo in sheep, including radiofrequency ablation [15]–[17].

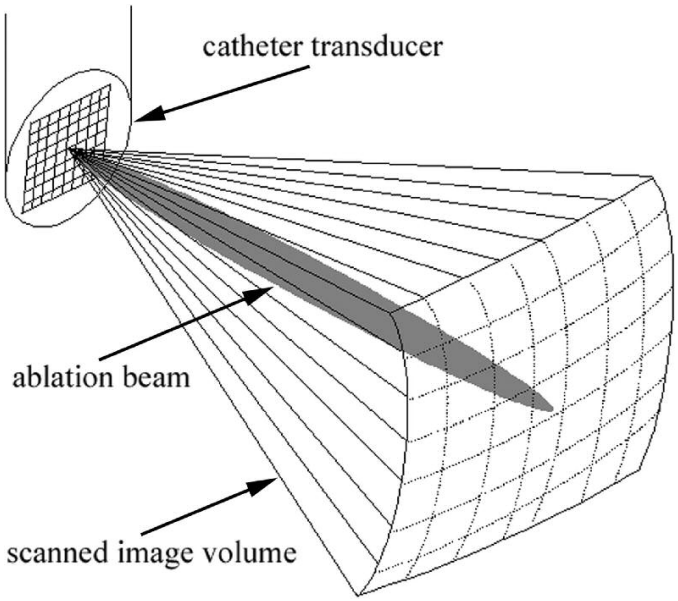

Fig. 1. A 2-D array at the distal end of an intracardiac catheter is used for real-time, 3-D imaging. An ablation transducer of one or more piezoelectric elements is used to form lesions in the myocardium.

We previously described two generations of integrated devices, a 12 Fr (outside diameter = 4.0 mm), side-viewing catheter with a 5 MHz imaging array adjacent to a 10 MHz ablation piston transducer and five integrated electrocardiogram electrodes [18], and a forward-viewing, 14 Fr (outside diameter = 4.5 mm) catheter [19], [20]. The latter device includes a 112-element, 5 MHz, 2-D array capable of real-time 3-D imaging. It has imaged wire targets and fixed ex vivo sheep hearts. Ablation is performed by a 10 MHz, PZT-4 ring transducer placed around the imaging array (Fig. 2). The ring has an outside diameter of 4.5 mm and an inside diameter of 3.1 mm. It is capable of producing temporal-average intensity (I_{TA}) of 16 W/cm^2 at an axial distance of 20 mm in water. A 2 minute ablation with this ring produced lesions in bovine muscle.

Manuscript received September 17, 2004; accepted February 1, 2005.

The authors are with the Department of Biomedical Engineering, Duke University, Durham, NC (e-mail: ken.gentry@duke.edu).

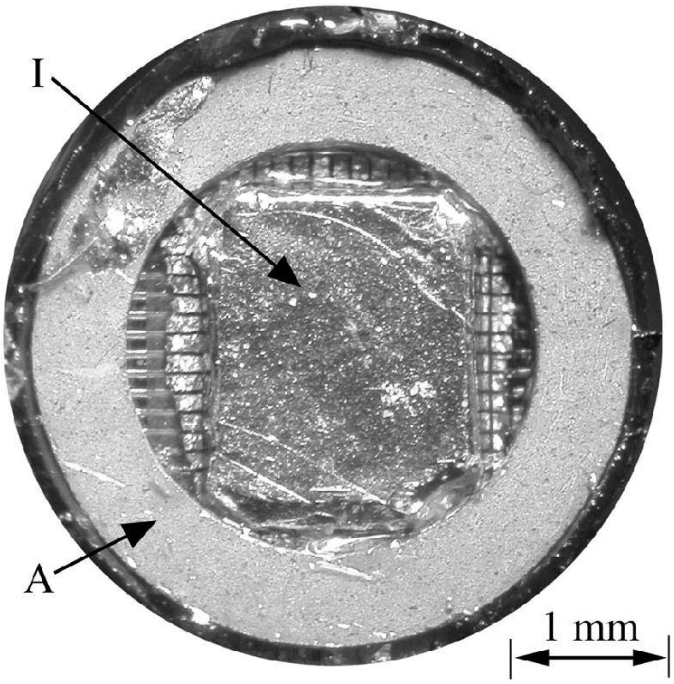

Fig. 2. The ring transducer to be modeled. A, ablation ring; I, imaging array.

In this work we present a method for modeling the lesions created by the ring transducer. After presenting the method, we validate it by comparing both the temperature rise and lesion size it predicts to experimental results. We then use the model to predict the ability of a new catheter ultrasound ablation device to create lesions in the myocardium. The 112-element, 2-D imaging array is retained in the new device because of its proven use in echocardiography [21], but it is embedded in a 1-D phased array for lesion creation. After examination of simulation results of this ablation array, we discuss the accuracy of our model as well as the problems that might be encountered when applying it.

II. Methods

A. Modeling

1. Simulation of Acoustic Intensity and Heat Production: Acoustic heating occurs when the sound field produced by a transducer is absorbed by the tissue. For a plane traveling wave, the volumetric heat generation rate (q_v, W/cm^3) is proportional to both the tissue's absorption and the intensity of the sound:

$$q_v = 2\alpha I_{TA}, \tag{1}$$

where α is the absorption (Np/cm), and I_{TA} is the intensity (W/cm^2) [22]. Throughout this paper, tissue absorption is assumed to equal tissue attenuation, experimental values for which are much more widely reported in the literature. In our model, the Field II program (version 3.0) [23] is used to calculate ultrasound intensity at the nodes of a 3-D finite-element mesh. The intensities are thresholded at 2% of the maximum (to reduce computation times), then are normalized to an experimentally measured intensity. The volumetric heat generation rate for a single, finite element is calculated from the average of the intensity at each of the element's eight nodes. Table I shows the values for absorption and other thermal properties used in our simulations [24], [25].

TABLE I
Acoustic and Thermal Properties.

Material or tissue	Tissue absorption (dB/cm/MHz)	Conductivity (W/cm/°C)	Heat capacity (J/cm^3/°C)
Water	0.0165	0.0060	4.2
Blood	0.20	0.0060	4.2
Bovine muscle	0.50	0.0053	3.4
Human heart	0.50	0.0050	3.7
PZT	—	0.0145	3.4

2. Finite-Element Modeling of Temperture Rise: To determine the temperature rise (T, °C) in tissue caused by this heat generation, the bio-heat transfer equation (neglecting perfusion) [5], [26] is solved:

$$\dot{T} = \frac{K}{c_v}\nabla^2 T + \frac{q_v}{c_v}, \tag{2}$$

where K is the thermal conductivity (W/cm/°C) and c_v is the volumetric heat capacity (J/cm^3/°C). Our model uses the FEA program LS-DYNA3D (Livermore Software Technology Corporation, Livermore, CA) using a time-domain explicit solver. Finite-element meshes for both the ring transducer and linear phased arrays were produced using LS-PREPOST (Livermore Software Technology Corporation, Livermore, CA). The simulations were allowed to run for 120 seconds (with a time step of 2 seconds) so the meshes were made large to allow for heat diffusion.

3. Calculation of Thermal Dose and Lesion Size: The size of the lesion produced by the temperature rise can be estimated using the concept of thermal dose [8], [27]. The temperature-time curve at each node is converted to equivalent minutes at the reference temperature of 43°C (t_{43}) with the following equation:

$$t_{43} = \sum_{t=0}^{t=final} R^{43-(T+T_a)}\Delta t, \tag{3}$$

where Δt is the time step in minutes and T is the temperature rise above T_a, the initial tissue temperature, at each time t. R is the so-called iso-dose constant and has been experimentally determined to equal 0.25 for temperatures less than the reference and 0.5 for temperatures greater than the reference across a range of tissue types [27]. For this model, a thermal dose greater than 240 minutes at any node was presumed to produce a lesion [8].

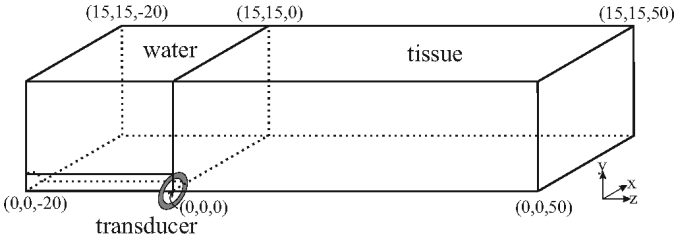

Fig. 3. Geometry used in the ring transducer model. The FEA nodal spacing is 0.5 mm. The thermal properties of the materials can be found in Table I. Ultrasound propagates in the $+z$ direction.

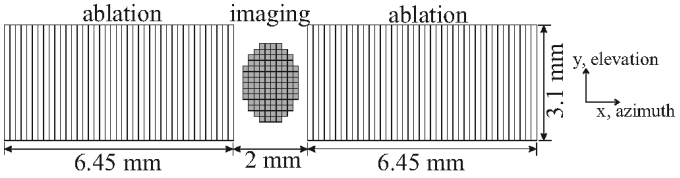

Fig. 4. A schematic of the proposed next generation device. A 112-element, 2-D array is to be used for 3-D ultrasound imaging. Forty-three elements of an 86-element, linear ablation array are placed on either side of the imaging array.

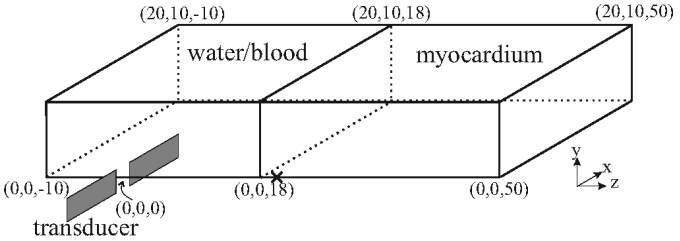

Fig. 5. Geometry used in the next generation linear-array transducer model. The nodal spacing is 0.5 mm. The thermal properties of the materials can be found in Table I. Ultrasound propagates in the $+z$ direction and is focused at (0,0,20) mm (marked by an **x**).

B. Ring Transducer Model Validation

To validate our model, we compared its results to the experiment. The ring transducer was used to create four lesions in bovine muscle. The tissue was 22-mm thick and placed on top of absorbing rubber in a room temperature (22°C) water bath. A signal source (8165A, Hewlett Packard, Palo Alto, CA) and radio frequency (RF) power amplifier (325LA, ENI, Rochester, NY) produced 500 cycle bursts at 10.1 MHz with a pulse repetition frequency of 9.8 kHz. A power meter (NRT, Rohde and Schwartz, Munich, Germany) measured forward (3.5 W) and reflected power (0.9 W) during the ablations. The ring transducer was placed just in contact with the tissue, and power was applied for 2 minutes. During three of these experiments, type-T thermocouples (0.127-mm diameter wire, 5TC-TT-T-36-36, Omega Engineering, Stamford, CT) were used to record tissue temperature versus time. In all, 13 temperature versus time curves were recorded during the three experiments. Following the 2-minute ablations, the tissue was sliced and lesion depth and diameter were determined by visual inspection.

The acoustic field from the ring transducer was modeled in Field II with 20% bandwidth Gaussian pulse impulse response input. The intensity from Field II was normalized to the value of 1.35 W/cm^2 at 20 mm. This is the derated value ($\alpha = 0.5$ dB/cm/MHz) of the intensity measured in water with a calibrated membrane PVDF hydrophone (Model 804, Sonic Technologies, Hatboro, PA) just prior to ablation. The geometry used for the ring transducer model is shown in Fig. 3. The transducer is centered at the origin, and the mesh extends from -20 to 50 mm in the z direction and 0 to 15 mm in the x and y directions. Nodal spacing is 0.5 mm, and ultrasound propagates in the $+z$ direction. Only one-quarter of the field is modeled to speed computation times. The self-heating of the transducer is included in the model as constant $q_v = 220$ W/m^3 in eight elements in a quarter ring around the origin. This was derived from the Krimholtz, Leedom, and Matthaei (KLM) model showing losses of 0.88 W in the piezoelectric ring (PiezoCAD, Sonic Concepts, Woodinville, WA) [28].

After FEA, temperature versus time curves from the thermocouples were compared to curves at nodes corresponding to the positions of the thermocouples. Additionally, the thermal dose was calculated using (3), and the simulated lesion depth and diameter were compared to averages from the four experimental lesions.

C. Design of Linear Phased Arrays

The model was used to aid in designing linear phased arrays for ablation. With our current cabling technology, a 10 Fr (outside diameter = 3.3 mm) catheter lumen can accommodate 198 channels. With 112 channels needed for the imaging array, 86 channels remain for the linear array. We have placed 43 ablation elements on either side of the imaging array (Fig. 4). Each linear-array element has a height of 3.1 mm and a pitch of 0.15 mm, and operates at 7.5 MHz. As opposed to the ring transducer that was in contact with the tissue to be ablated, this array is designed to ablate myocardium from a distance. The finite-element mesh used to model the linear ablation array when focused on-axis at 20 mm is again a quarter model with nodal spacing of 0.5 mm (Fig. 5). The mesh extends from -10 to 50 mm in the z direction, 0 to 20 mm in the x direction, and 0 to 10 mm in the y direction for a total of 101,481 nodes. The mesh is modeled as either water or blood for z less than 18 mm and as myocardium for z greater than 18 mm.

We also simulated the effect of focusing the ablation beam off-axis at $x = 10$ mm, $y = 0$ mm, and $z = 20$ mm. The acoustic heat generation is no longer symmetric in azimuth, so a half symmetry model is used (Fig. 6). The mesh extends from -10 to 50 mm in the z direction, -30 to 30 mm in the x direction, and 0 to 10 mm in the y direction for a total of 307,461 nodes. No transducer self-heating was included in the linear phased-array simulations because the transducer is not in contact with the myocardium.

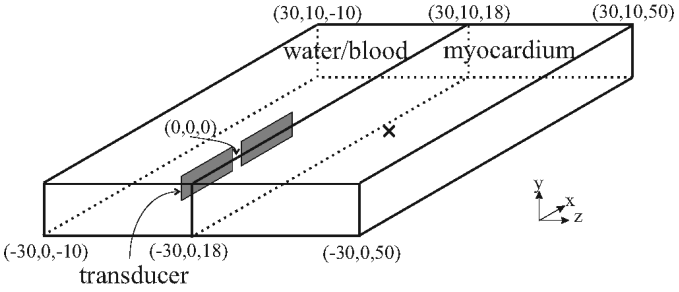

Fig. 6. Geometry used in the next generation linear-array transducer model when the acoustic field is steered off-axis to (10,0,20) mm (marked by an **x**). The nodal spacing is 0.5 mm. The thermal properties of the materials can be found in Table I. Ultrasound propagates in the $+z$ direction.

The effects on I_{TA} due to three design variations were simulated. First, Field II was used to calculate the relative intensity change due to focusing the linear array in its elevation direction at $z = 20$ mm as from a PZT cylinder. Second, the KLM model was used to determine the effects on the amplitude of the impulse response from individual array elements due to using a triple-layer PZT-4 rather than single-layer material. Triple-layer material has improved electrical matching, and in the KLM model it is approximated by a single-layer material in series with an ideal transformer with a turns ratio of 1:3. These impulse responses were used as Field II input to see the increase achieved in intensity. Third, the effects of transmitting through a water-filled balloon rather than blood [29], were studied. The effects of the balloon membrane were not included. All permutations of these three changes, for a total of eight linear-array designs, were simulated with the beam focused on-axis and again for off-axis focusing. All intensity values were scaled assuming a baseline value of 25 W/cm^2 at the focus for the nonelevation-focused, single-layer transducer steered on-axis in blood. The baseline value was extrapolated from experiments with a prototype 35-element, linear-phased array.

III. Results

A. Validation of Ring Transducer Model

1. Intensity and Temperature Rise: The I_{TA} from the ring transducer, as calculated by Field II then scaled, is shown in Fig. 7. The maximum intensity in tissue was 7.45 W/cm^2 at (0,0,3) mm. The simulated temperature rise after a 2-minute ablation is shown in Fig. 8. Part of the xz plane is shown and mirrored about the x axis. The maximum temperature rise in tissue was 42.6°C.

Temperature rise versus time curves for the three thermocouples in a typical ablation trial are shown in Fig. 9 and are compared to FEA results. The thermocouples were placed at the positions shown on the graph. The average absolute difference between final experimental temperature rise and final FEA temperature rise for all 13 thermocouples in the three trials was 1.95 ± 0.72°C. The FEA

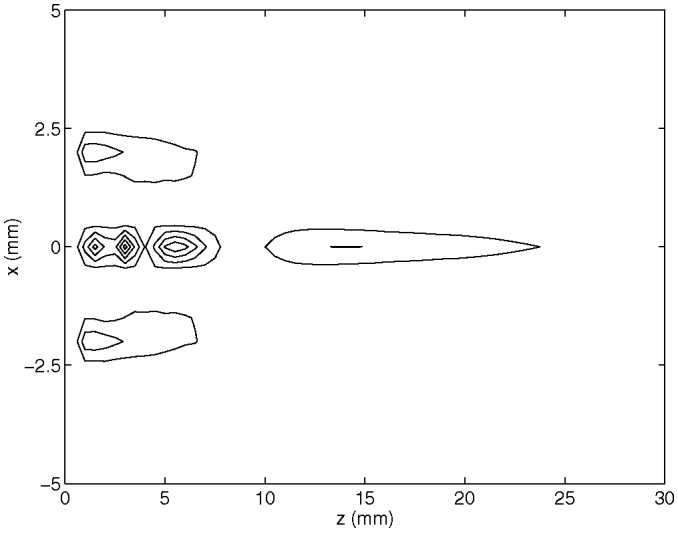

Fig. 7. I_{TA} in tissue in the azimuthal plane is shown. The intensity values have been scaled to a value of 1.35 W/cm^2 at an on-axis distance of 20 mm. This value is derated at 0.5 dB/cm/MHz from a measured I_{TA} of 13.5 W/cm^2 in water. The contours are at 10%, 30%, 50%, 70%, and 90% of the maximum value.

underestimated the final temperature rise at 11 positions and overestimated final temperature rise at the other two.

2. Thermal Dose and Lesion Size: The thermal dose was calculated using (3). The lesion outlined by those nodes with a thermal dose greater than 240 minutes had a depth of 1.75 mm and a diameter of 5.50 mm. The average depth and diameter of the four experimental lesions was 1.75 ± 0.24 mm and 4.56 ± 0.56 mm, respectively.

B. Linear Phased Arrays

By using a fixed elevation focus, I_{TA} was increased 1.2 times over a flat transducer. The KLM model indicated that a triple-layer PZT-4 element would produce a transmit pressure 2.8 times that of the single-layer element. This increased I_{TA} 7.7 times. And, by transmitting through a water-filled balloon rather than blood, I_{TA} is increased 1.7 times. Fig. 10 shows relative contour plots of intensity from Field II in the azimuth dimension for the arrays transmitting through blood and water, both on- and off-axis. These relative plots of intensity are scaled to find the actual intensity used in the FEA simulations. Temperature rise scales quite well with intensity and temperature rise contour maps for similar transducer configurations are nearly identical. Thus we show only four temperature rise contour maps, one each for the baseline array transmitting through blood and water, both on- and off-axis (Fig. 11). Temperature rise versus time curves at the focus for all transducer configurations are shown in Fig. 12. Table II compares the focal I_{TA} and the temperature rise at the focus after 120 seconds for all transducer configurations. Additionally it shows whether a lesion was produced in 2 minutes using the criterion of a thermal dose, t_{43}, of 240 minutes.

TABLE II
LINEAR PHASED ARRAY SIMULATION RESULTS.

	Focal I_{TA} (W/cm^2)		Focal temp. rise at 120 s (°C)		Lesion ?	
Transducer	on-axis	off-axis	on-axis	off-axis	on-axis	off-axis
Blood path						
Baseline	25.0	16.2	11.4	6.1	No	No
Curved	30.7	19.0	12.5	6.6	No	No
Triple-layer	192.9	124.7	88.0	47.0	Yes	Yes
Curved, triple-layer	237.7	147.2	96.5	50.2	Yes	Yes
Water path						
Baseline	42.1	27.9	18.4	10.0	Yes	No
Curved	51.8	32.9	20.3	10.8	Yes	No
Triple-layer	325.7	216.3	142.2	77.0	Yes	Yes
Curved, triple-layer	402.2	256.0	156.8	82.9	Yes	Yes

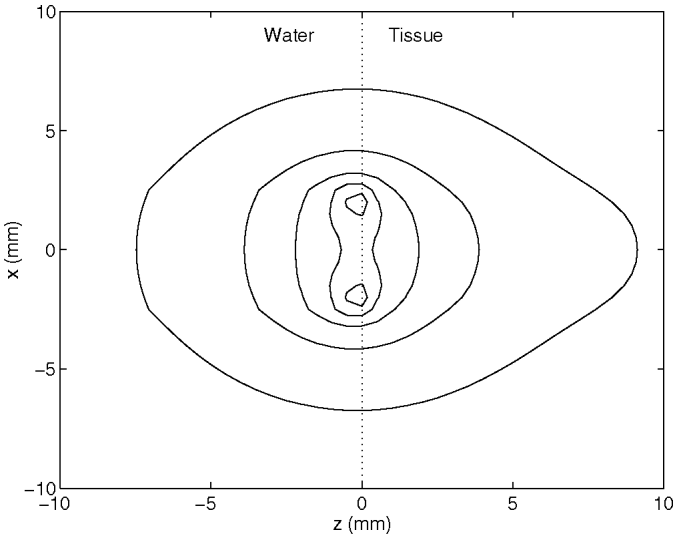

Fig. 8. The temperature rise at the end of a 2-minute ablation with the ring in the xz plane. The contours are at 10%, 30%, 50%, 70%, and 90% of the maximum temperature rise of 52°C. This maximum temperature rise occurred in the transducer PZT. The maximum temperature rise in tissue was 42.6°C. The movie shows the temperature rise as it changes over the 2 minutes.

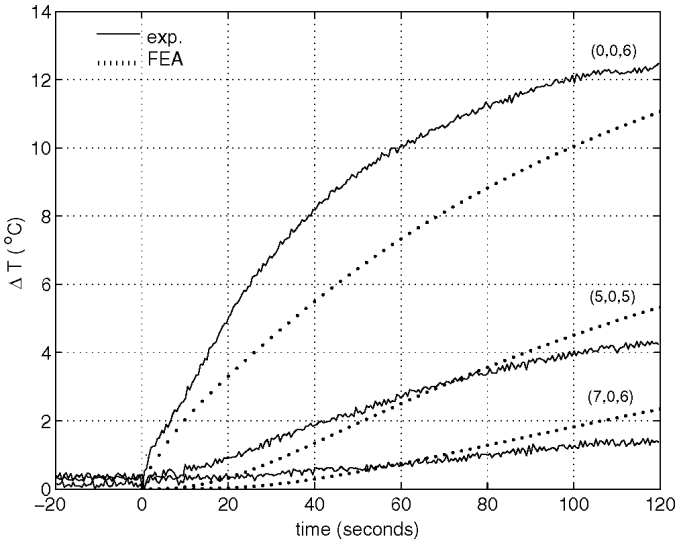

Fig. 9. The temperature rise measured from three thermocouples during a typical ablation trial (solid lines) is compared to FEA results (dotted lines). The thermocouples were positioned at the (x, y, z) positions indicated on the graph.

IV. DISCUSSION

A. Model Validation

Our model successfully predicted the temperature rise from the ring transducer to within 2°C. The differences between experimental and FEA data may be caused by inaccuracies in the experiment or the model. The largest experimental uncertainty was in the placement of the thermocouple tips in the tissue. The temperature gradient in the ablation site from the unfocused ring is steep in both the axial and radial directions, and the thermocouples could be placed with a precision of ±2 mm. The errors caused by misplaced thermocouple leads might be expected to be equally likely to be positive or negative. However, 11 of the 13 thermocouples measured a temperature rise greater than that predicted by the model, so this error is probably small in comparison to modeling errors or thermal measurement artifacts. No attempt was made to compensate for possible overestimation of temperature due to viscous shearing of the thermocouples.

Many types of errors may have occurred when modeling the temperature rise from the ring transducer. The most obvious is the common problem of inaccurate tissue properties as Field II or FEA model input. We have found that changing α, K, or c_v by 20% can alter the predicted temperature rise after 2 minutes by more than 10% (depending on the axial and radial distance from the transducer). Additionally, because the transducer was in contact with the lesion site, it was necessary to include transducer self-heating in the model. Without it, the modeled temperature rise at the end of two minutes was approximately half the measured temperature rise. We included transducer

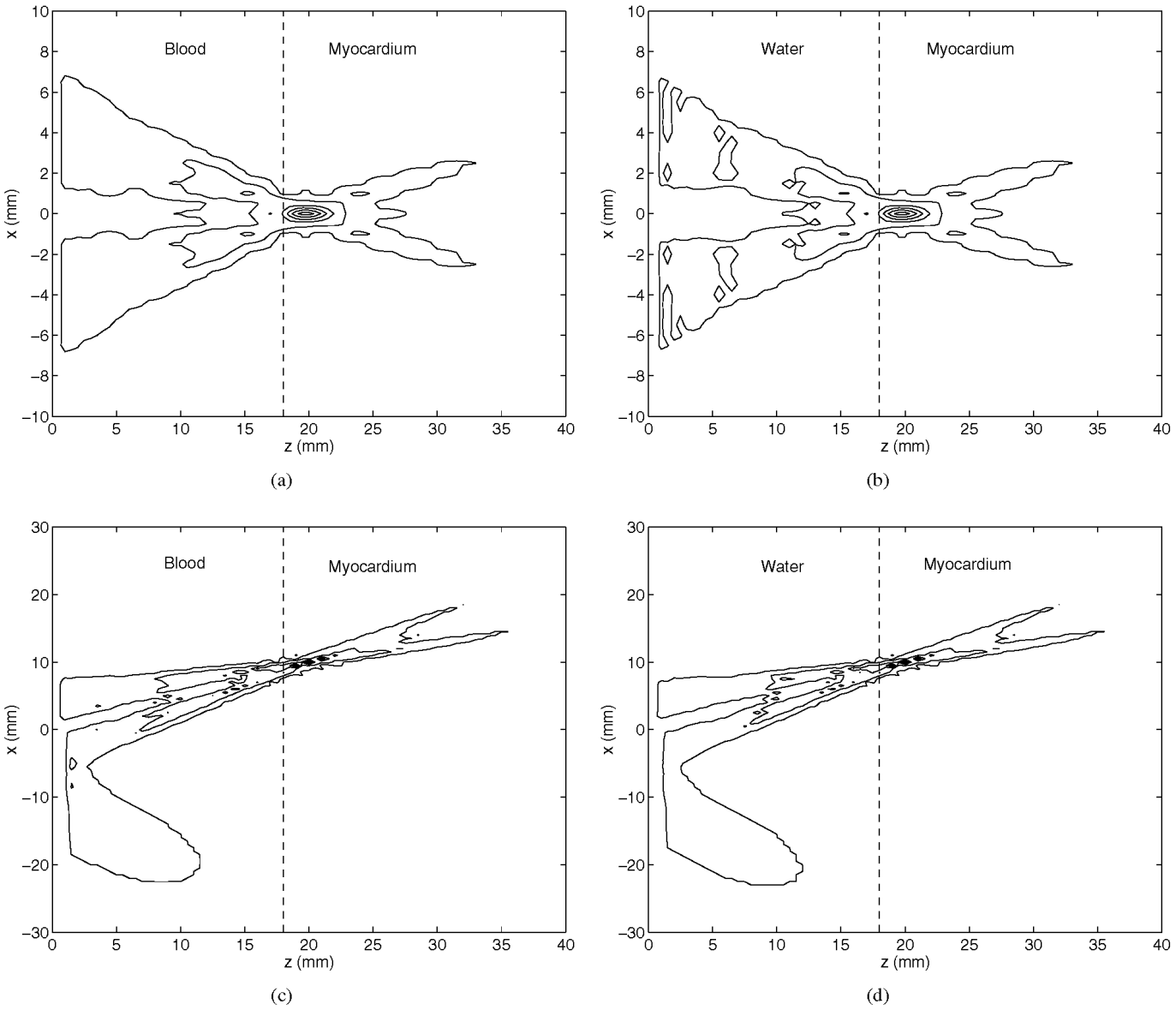

Fig. 10. Intensity in the azimuth plane for the linear phased arrays focused on-axis through blood (a), on-axis through water (b), off-axis through blood (c), and off-axis through water (d). Contours are at 10%, 30%, 50%, 70%, and 90% of maximum. Note different ordinate scales.

self-heating as constant heat sources at the position of the ring transducer with magnitude found from KLM analysis. A more accurate model might more directly measure the power lost in the transducer as heat.

The thermal dose concept is extremely powerful when comparing various temperature versus time curves and computing lesion size. The model predicted lesion depth very well, but underestimated lesion diameter by 20%. The longer axes of the experimental lesions more closely matched the diameter of the modeled lesion. The ring transducer may not have been transmitting a radially symmetric acoustic beam, or the tissue may have been thermally anisotropic, allowing heat to conduct more readily in one dimension. Overall, however, our experiments have shown the usefulness of this model as a tool in predicting lesion formation from ultrasound transducers.

B. Linear Phased-Array Designs

Our results show that creating lesions in the myocardium from an array transducer in a catheter may be possible, even given our restraints on channel count and aperture size. The baseline array transmitting through blood is inadequate. Therefore, it is necessary to increase the amount of acoustic intensity at the focus by some other means. From our results, it appears that our transducer design alternatives would produce enough power, both on- and off-axis, to create a lesion.

Note that these simulations do not predict what factors ultimately might limit the I_{TA} and thus the temperature rise, particularly as the intensity increases. The piezoelectric material itself may saturate at power levels lower than those needed to produce higher intensities. At these higher

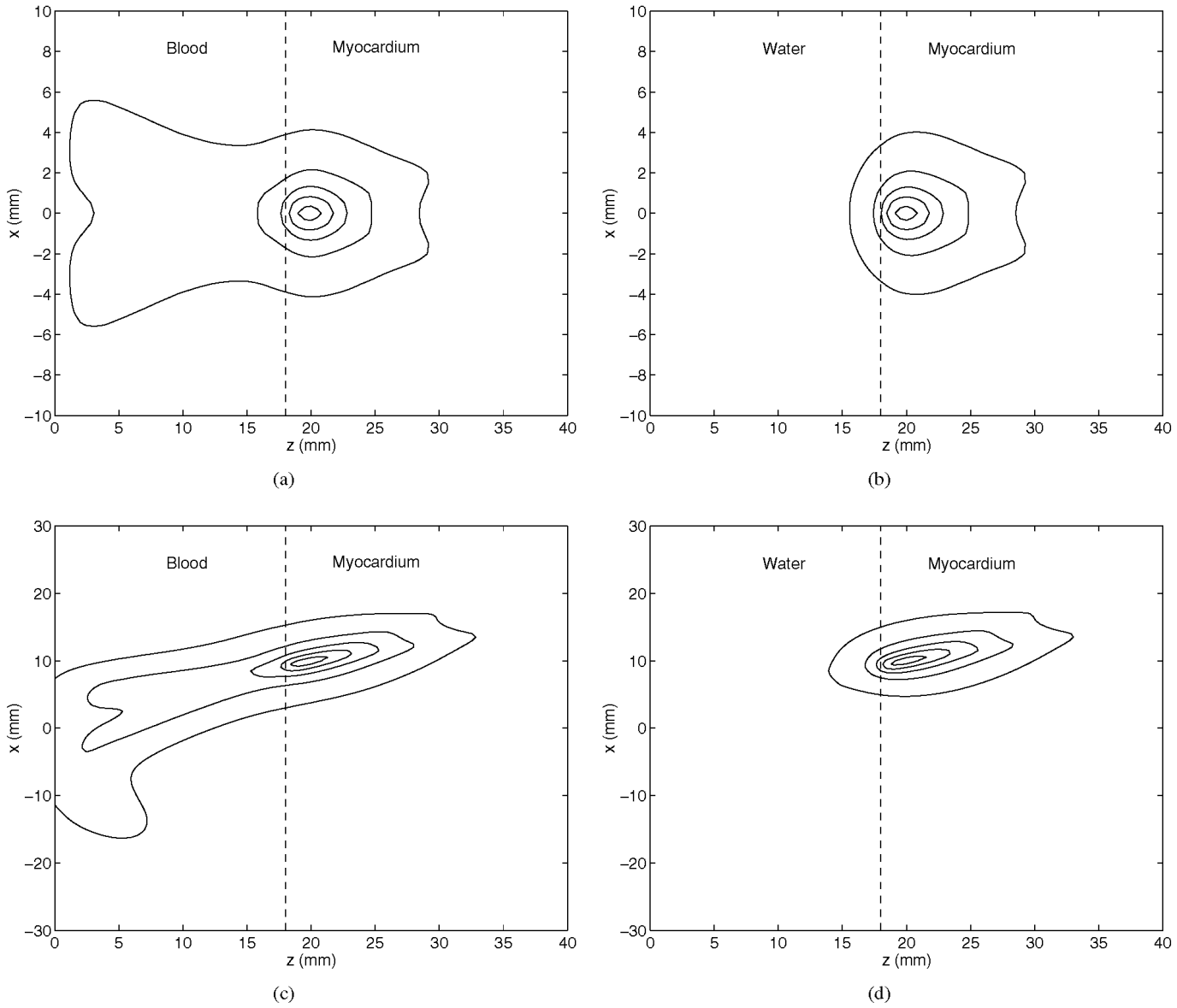

Fig. 11. Temperature rise at 120 seconds for the linear phased arrays focused on-axis through blood (a), on-axis through water (b), off-axis through blood (c), and off-axis through water (d). Contours are at 10%, 30%, 50%, 70%, and 90% of maximum. Note different ordinate scales.

power levels, the transducer may experience self-heating (as the ring transducer did) large enough to damage the device. Additionally, there are limits to the amount of electrical power that a phased-array ultrasound scanner can produce safely. Conversely, at higher power levels, the prefocal temperature rise is expected to increase due to nonlinear acoustic propagation [30].

In order to accurately predict lesion size from the linear phased arrays, it may be necessary to improve our modeling of the anatomy of the left atrium. We do not include the cooling effects of the pumping blood on the heart surface, nor do we accurately model the thickness of the left atrial wall. In reality, the tissue to be lesioned is 2–5 mm thick, not several centimeters as in our model. The presence of other tissue types behind the heart wall may affect the temperature rise at the focus. Other considerations include the effects of myocardial movement and changes in tissue properties during the cardiac cycle. It may be necessary to lodge the catheter in a stable position relative to the target cardiac structure. One possibility is to lodge the catheter in coronary sinus as shown by Lee *et al.* [17]. Another option is to gate the therapy pulses in synchrony with an electrocardiogram. And, by neglecting myocardial perfusion in the bio-heat transfer equation we may be ignoring a significant source of tissue cooling.

Acknowledgment

This work was supported by NSF grant DMR 0104304.

References

[1] J. E. Zimmer, K. Hynynen, D. S. He, and F. Marcus, "The feasibility of using ultrasound for cardiac ablation," *IEEE Trans. Biomed. Eng.*, vol. 42, pp. 891–897, Sep. 1995.

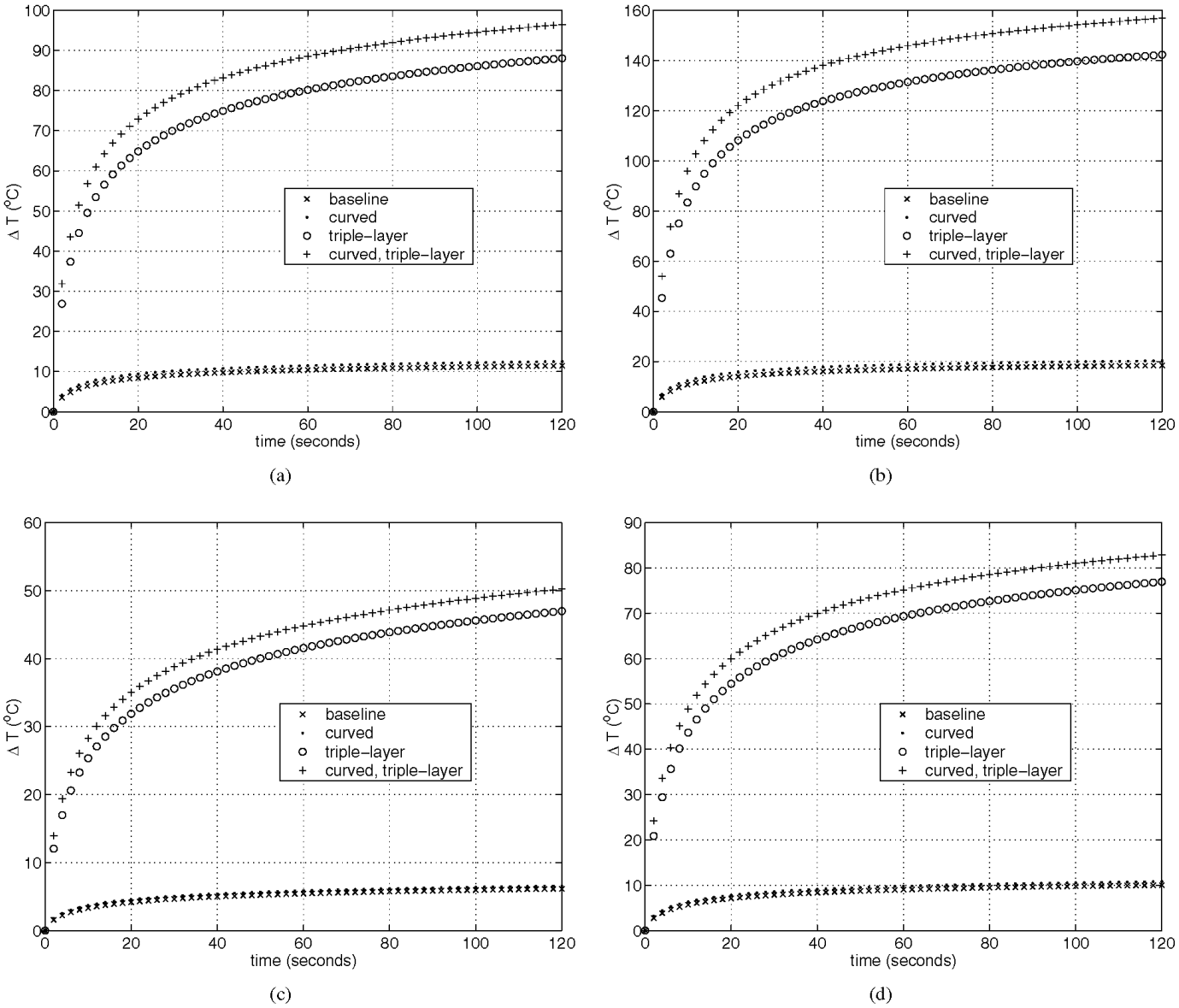

Fig. 12. Focal temperature rise versus time curves for the linear phased arrays focused on-axis through blood (a), on-axis through water (b), off-axis through blood (c), and off-axis through water (d). Note different ordinate scales.

[2] K. Hynynen, J. Dennie, J. E. Zimmer, W. N. Simmons, D. S. He, F. I. Marcus, and M. Aguirre, "Cylindrical ultrasonic transducers for cardiac catheter ablation," *IEEE Trans. Ultrason., Ferroelect., Freq. Contr.*, vol. 44, pp. 144–151, Feb. 1997.

[3] T. Ohkubo, K. Okishige, Y. Goseki, T. Maysubara, K. Hiejima, and C. Ibukiyama, "Experimental study of catheter ablation using ultrasound energy in canine and porcine hearts," *Jpn. Heart J.*, vol. 39, pp. 399–409, May 1998.

[4] M. D. Lesh, P. G. Guerra, F. X. Roithinger, Y. Goseki, P. B. Sparks, C. Diedrich, W. H. Nau, M. Maguire, and K. Taylor, "Novel catheter technology for ablative cure of atrial fibrillation," *J. Interv. Cardiol. Electron.*, vol. 4, pp. 127–139, Jan. 2000.

[5] W. L. Nyborg, "Solutions of the bioheat transfer equation," *Phys. Med. Biol.*, vol. 33, pp. 785–792, July 1988.

[6] J. Wu and G. Du, "Temperature elevation generated by a focused Gaussian beam of ultrasound," *Ultrasound Med. Biol.*, vol. 16, no. 5, pp. 489–498, 1990.

[7] A. K. Chan, R. A. Sigelman, A. W. Guy, and J. F. Lehmann, "Calculation by the method of finite differences of the temperature distribution in layered tissues," *IEEE Trans. Biomed. Eng.*, vol. BME-20, no. 2, pp. 86–90, Mar. 1973.

[8] C. A. Damianou, K. Hynynen, and X. Fan, "Evaluation of accuracy of a theoretical model for predicting the necrosed tissue volume during focused ultrasound surgery," *IEEE Trans. Ultrason., Ferroelect., Freq. Contr.*, vol. 42, pp. 182–187, Mar. 1995.

[9] M. L. Palmeri and K. R. Nightingale, "On the thermal effects associated with radiation force imaging of soft tissue," *IEEE Trans. Ultrason., Ferroelect., Freq. Contr.*, vol. 51, pp. 551–565, May 2004.

[10] S. W. Smith, H. G. Pavy, and O. T. von Ramm, "High-speed ultrasound volumetric imaging system—Part I: Transducer design and beam steering," *IEEE Trans. Ultrason., Ferroelect., Freq. Contr.*, vol. 38, pp. 100–108, Mar. 1991.

[11] O. T. von Ramm, S. W. Smith, and H. G. Pavy, "High-speed ultrasound volumetric imaging system—Part II: Parallel processing and image display," *IEEE Trans. Ultrason., Ferroelect., Freq. Contr.*, vol. 38, pp. 109–115, Mar. 1991.

[12] I. D. McRury and D. E. Haines, "Ablation for the treatment of arrhythmias," *Proc. IEEE*, vol. 84, pp. 404–416, Mar. 1996.

[13] J. B. Morton, P. Sanders, M. J. Byrne, J. Power, C. Mow, G. A. Edwards, and J. M. Kalman, "Phased-array intracardiac echocardiography to guide radiofrequency ablation in the left

atrium and at the pulmonary vein ostium," *J. Cardiovasc. Electron.*, vol. 12, pp. 343–348, Mar. 2001.
[14] J. M. Mangrum, J. P. Mounsey, L. C. Kok, J. P. DiMarco, and D. E. Haines, "Intracardiac echocardiography-guided, anatomically based radiofrequency ablation of focal atrial fibrillation originating from pulmonary veins," *J. Amer. Coll. Cardiol.*, vol. 39, pp. 1964–1972, June 2002.
[15] S. W. Smith, E. D. Light, S. F. Idriss, and P. D. Wolf, "Feasibility study of real-time three-dimensional intracardiac echocardiography for guidance of interventional electrophysiology," *PACE*, vol. 25, pp. 351–357, Mar. 2002.
[16] E. D. Light, S. F. Idriss, P. D. Wolf, and S. W. Smith, "Real-time three-dimensional intracardiac echocardiography," *Ultrasound Med. Biol.*, vol. 27, pp. 1177–1183, Sep. 2001.
[17] W. Lee, S. F. Idriss, P. D. Wolf, and S. W. Smith, "A miniaturized catheter 2-D array for real-time, 3-D intracardiac echocardiography," *IEEE Trans. Ultrason., Ferroelect., Freq. Contr.*, vol. 51, pp. 1334–1346, Oct. 2004.
[18] K. L. Gentry, E. D. Light, and S. W. Smith, "Combined 3-D intracardiac echo and ultrasound ablation," in *Proc. SPIE Med. Imaging: Ultrason. Imaging Signal Processing*, Feb. 2003, pp. 166–173.
[19] K. L. Gentry and S. W. Smith, "Integrated catheter for 3-D intracardiac echocardiography and ultrasound ablation," presented at *Proc. IEEE Ultrason. Symp.*, Oct. 2003, pp. 1099–1102.
[20] K. L. Gentry and S. W. Smith, "Integrated catheter for 3-D intracardiac echocardiography and ultrasound ablation," *IEEE Trans. Ultrason., Ferroelect., Freq. Contr.*, vol. 51, pp. 800–808, July 2004.
[21] W. Lee, S. F. Idriss, P. D. Wolf, and S. W. Smith, "Dual lumen transducer probes for real-time 3-D interventional cardiac ultrasound," *Ultrasound Med. Biol.*, vol. 29, pp. 1297–1304, Sep. 2003.
[22] Exposure Criteria for Medical Diagnostic Ultrasound: I. Criteria Based on Thermal Mechanisms. National Council on Radiation Protection and Measurement, Bethesda, MD, Report No. 113, 1992.
[23] J. A. Jensen and N. B. Svendsen, "Calculation of pressure fields from arbitrarily shaped, apodized, and excited ultrasound transducers," *IEEE Trans. Ultrason., Ferroelect., Freq. Contr.*, vol. 39, pp. 262–267, Mar. 1992.
[24] F. A. Duck, *Physical Properties of Tissue*. London: Academic, 1990.
[25] Technical data, Jun. 2004, Bloomingdale, IL: CTS Corporation, http://www.ctscorp.com/components/Datasheets/PZT.pdf.
[26] H. H. Pennes, "Analysis of tissue and arterial blood temperatures in the resting human forearm," *J. Appl. Phys.*, vol. 1, pp. 93–122, Aug. 1948.
[27] S. A. Sapareto and W. C. Dewey, "Thermal dose determination in cancer therapy," *Int. J. Radiat. Oncol.*, vol. 10, pp. 787–800, June 1984.
[28] R. Krimholtz, D. A. Leedom, and G. L. Matthaei, "New equivalent circuits for elementary piezoelectric transducers," *Electron. Lett.*, vol. 6, pp. 398–399, 1970.
[29] A. Natale, E. Pisano, J. Shewchik, D. Bash, R. Fanelli, D. Potenza, P. Santarelli, R. Schweikert, R. White, W. Saliba, L. Kanagaratnam, P. Tchou, and M. Lesh, "First human experience with pulmonary vein isolation using a through-the-balloon circumferential ultrasound ablation system for recurrent atrial fibrillation," *Circulation*, vol. 102, pp. 1879–1882, Oct. 2000.
[30] D. R. Bacon and E. L. Carstensen, "Increased heating by diagnostic ultrasound due to nonlinear propagation," *J. Acoust. Soc. Amer.*, vol. 88, pp. 26–34, July 1990.

Kenneth L. Gentry was born in Springfield, IL, on July 24, 1977. He received a B.S. degree in biomedical engineering from Marquette University, Milwaukee, WI, in 1999.

Currently, he is a biomedical engineering doctoral candidate at Duke University, Durham, NC. He currently researches the design and fabrication of intracardiac transducers for both real-time volumetric imaging and ultrasound ablation.

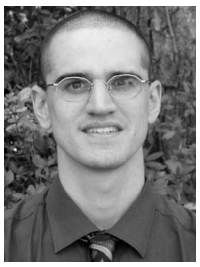

Mark L. Palmeri (S'99) received his B.S. degree (Biomedical and Electrical Engineering) in 2000 from Duke University. He is currently a student in the Medical Scientist Training Program and a James B. Duke graduate fellow in the Biomedical Engineering Department at Duke University.

Nasheer Sachedina was born on December 27, 1982, in Chicago, IL. He is currently majoring in biomedical engineering and electrical engineering at Duke University, Durham, NC. As a Pratt Engineering Undergraduate Fellow, he is modeling and building ultrasound transducers for ablation. Upon graduation he will be attending the University of Miami School of Medicine, Miami, FL.

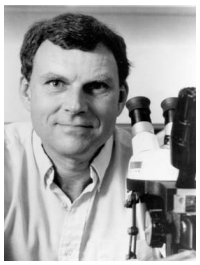

Stephen W. Smith (M'91) was born in Covington, KY, on July 27, 1947. He received the B.A. degree in physics (summa cum laude) in 1967 from Thomas More College, Ft. Mitchell, KY, the M.S. degree in physics in 1969 from Iowa State University, Ames, and the Ph.D. degree in biomedical engineering in 1975 from Duke University, Durham, NC.

In 1969, he became a Commissioned Officer in the U.S. Public Health Service, assigned to the Food and Drug Administration, Center for Devices and Radiological Health, Rockville, MD, where he worked until 1990 in the study of medical imaging, particularly diagnostic ultrasound and in the development of performance standards for such equipment. In 1978, he became an adjunct associate professor of radiology at Duke University Medical Center. In 1990, he became an associate professor of biomedical engineering and radiology, and Director of Undergraduate Studies in Biomedical Engineering at Duke University. He holds 16 patents in medical ultrasound and has authored 100+ publications in the field.

Dr. Smith is cofounder of Volumetrics Medical Imaging. He has served on the education committee of the American Institute of Ultrasound in Medicine, the executive board of the American Registry of Diagnostic Medical Sonographers, the editorial board of *Ultrasonic Imaging*, and the Technical Program Committee of IEEE-UFFC. He was corecipient of the American Institute of Ultrasound in Medicine Matzuk Award in 1988 and 1990 and corecipient of the IEEE-UFFC Outstanding Paper Award in 1983 and 1994.